# Laterally screened two-dimensional plasma excitations in a disk-shaped two-dimensional electron system

A. M. Zarezin,[1] P. A. Gusikhin,[1] A. A. Zabolotnykh,[2] A. S. Astrakhantseva,[1] I. V. Kukushkin,[1] and V. M. Muravev[1]
[1]*Institute of Solid State Physics, RAS, Chernogolovka 142432, Russia*
[2]*Kotelnikov Institute of Radio-Engineering and Electronics of the RAS, Mokhovaya 11-7, Moscow 125009, Russia*

(Received 28 May 2023; revised 15 August 2023; accepted 1 September 2023; published 14 September 2023)

We investigated plasma excitations in a disk-shaped two-dimensional electron system (2DES) laterally screened by a coplanar metal electrode surrounding the 2DES with a fixed-size separation gap around the perimeter of the disk. We find that lateral screening leads to a significant redshift in the plasmon frequency as the gap width approaches zero. It is caused by the redistribution of charges in the metallic gate that induce a logarithmic screening potential in the 2DES region. The spectroscopy of laterally screened plasmons provides valuable information on the structure of the 2DES edge. We developed a theoretical model and performed numerical simulations which show good agreement with the experimental data.

DOI: 10.1103/PhysRevB.108.115419

The study of plasma excitations in two-dimensional electronic systems (2DES) has been attracting considerable interest for more than 50 years [1–5]. One of the main reasons is that the plasmonic response governs the operation of all semiconductor devices in the terahertz frequency range. Therefore, the development of terahertz electronics requires the understanding of two-dimensional (2D) plasmonics at the most fundamental level. The spectrum of 2D plasmons has been well established both theoretically [6] and experimentally [7–9] as follows:

$$\omega_p(q) = \sqrt{\frac{ne^2 q}{2m^*\varepsilon_0\varepsilon(q)}}, \qquad (q \gg \omega/c). \tag{1}$$

Here, $q$ is the plasmon wave vector, $n$ and $m^*$ are the density and effective mass of the 2DES electrons, while $\varepsilon_0$ and $\varepsilon(q)$ denote the vacuum permittivity and the effective permittivity of the surrounding medium. One of the most attractive properties of 2D plasmons is that their frequency can be tuned over a wide range by varying the electron density. Usually, it is accomplished by evaporating a gate on top of the crystal at a distance $a$ above the 2DES.

For the gated 2DES, the plasmon dispersion in Eq. (1) becomes linear due to the strong modification of the Coulomb interaction between the charge fluctuations, which can be accounted for by the effective dielectric function $\varepsilon(q) = 1/2qa$ [10]. However, such a type of gating is not very practical in plasmonics as the gate screens the incident electromagnetic radiation, preventing the excitation of plasma waves in the 2DES. Therefore, lateral gates are more suitable for exciting and controlling the desired 2D plasma waves. Previous theoretical studies showed that lateral Coulomb screening leads to the redshift in the plasmon frequency, with no significant effect on the mode dissipation [11–15]. Regrettably, so far, there have been no systematic attempts made at the experimental investigation of laterally screened 2D plasma excitations.

In the present paper, we report on the resonant microwave absorption of a 2DES disk laterally screened by a metallic gate. Our experimental findings show that lateral screening produces a substantial redshift in the plasmon frequency as the gap between the 2DES and the gate is reduced. The redshift is the result of the redistribution of charges in the metallic gate, which induces a logarithmic screening potential in the 2DES disk. We demonstrate that spectroscopy of laterally screened plasmons offers a revealing insight into the structure of the 2DES edge. We propose a theoretical model and perform numerical simulations that are consistent with the experimental data.

The experiments were conducted on $Al_{0.24}Ga_{0.76}As/GaAs/Al_{0.24}Ga_{0.76}As$ heterostructures hosting a 2D electron system. In particular, we examine two types of structures. One, with a single 30-nm-wide quantum well 370 nm below the crystal surface, hosting a 2DES with the electron density $n = 1.6 \times 10^{11}\,\mathrm{cm}^{-2}$ and the electron mobility $\mu = 2 \times 10^6\,\mathrm{cm}^2/\mathrm{V}\cdot\mathrm{s}$ at $T = 4.2$ K. The other, with a 20 nm-wide quantum well 220-nm deep, having the 2DES electron density $n = 3.5 \times 10^{11}\,\mathrm{cm}^{-2}$ and the electron mobility $\mu = 0.4 \times 10^6\,\mathrm{cm}^2/\mathrm{V}\cdot\mathrm{s}$ at $T = 4.2$ K. The geometry of the structure under study is depicted in the top panel of Fig. 1. The samples were patterned by the E-beam lithography as follows. First, a disk-shaped mesa of diameter $d$ was fabricated from a 2DES to produce two sets of samples with $d = 0.25$ and 0.5 mm. Then, a 200 nm Au/Cr gate was thermally evaporated on top of the crystal in the form of a concentric ring, with a gap of the width $h$ separating the gate from the 2DES disk around the perimeter. The size of the gap varies between different samples, ranging from $h = 0.2$ μm to 40 μm. The sample was mounted at the center of a WR-28 rectangular waveguide used to feed the microwave radiation of 10–60 GHz. The generator power is adjusted to avoid sample overheating in the range 0.01–1 mW. Then, it is placed into a cryostat with a base temperature of 1.5 K, inside a superconducting coil producing a magnetic field $B$ of 0–7 T.

 

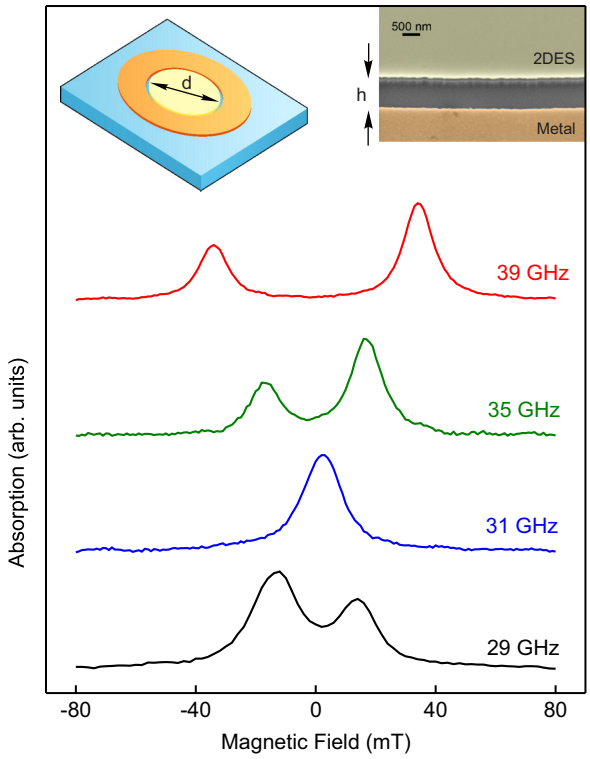


FIG. 1. (Top left) Schematic drawing of the experimental structure. A disk-shaped mesa marked in yellow is screened laterally by the coplanar metallic gate marked in orange. (Top right) SEM image of the sample edge with the gap width $h = 0.78$ μm. (Bottom panel) Microwave absorption dependence on the $B$ field, measured at indicated frequencies, for the sample with the 2DES diameter $d = 0.25$ mm, the gap width $h = 10$ μm, and the electron density $n = 1.6 \times 10^{11}$ cm$^{-2}$. The plots are offset for clarity.

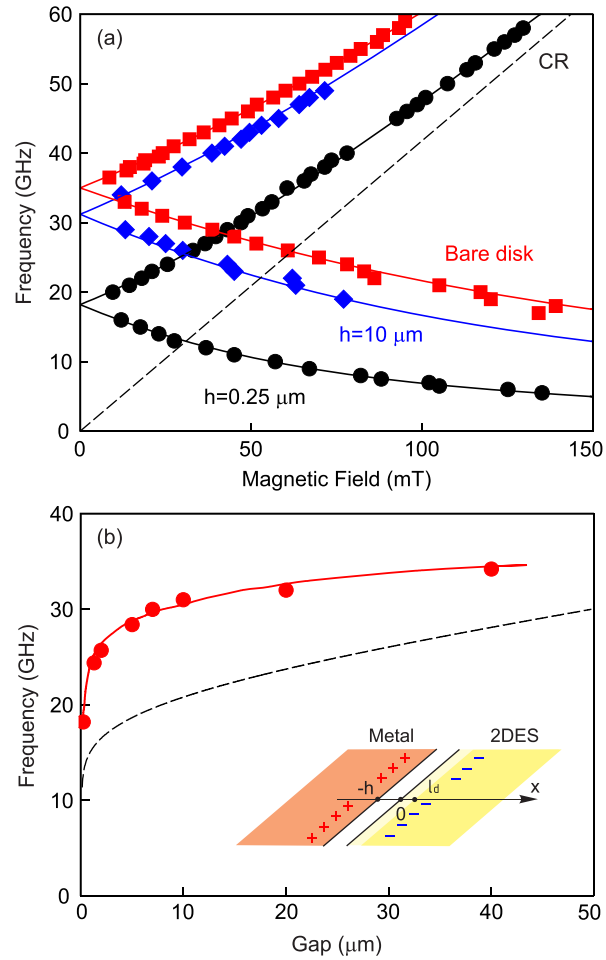


FIG. 2. (a) Magnetodispersion of the plasmon mode for the resonance observed in the 2DES with diameter $d = 0.25$ mm at the gap widths $h = 0.25$ μm (black dots) and 10 μm (blue diamonds). Red squares denote the data for the bare disk of the same diameter. The solid lines represent the curves calculated from Eq. (2). The dashed line indicates the cyclotron resonance $\omega_c = eB/m^*$. (b) Dependence of the plasmon frequency on the size of the gap between the 2DES and the gate. The measurements are plotted in red dots. The solid and dashed curves designate, respectively, the numerical simulation results and the prediction of the theoretical model (4). The inset depicts a close-up view of the gap area, showing the depletion region of size $l_d$ at the edge of the 2DES.

To detect the plasma excitations, we employ a nondestructive optical technique [16] based on the high sensitivity of the 2DES luminescence spectrum to the heating caused by the absorption of microwave radiation.

In Fig. 1, we display the microwave absorption versus the applied magnetic field, measured at 29, 31, 35, and 39 GHz. The data refer to the sample with the 2DES diameter $d = 0.25$ mm, the gap width $h = 10$ μm, and the electron density $n = 1.6 \times 10^{11}$ cm$^{-2}$. These results show that absorption curves have a well-resolved resonance corresponding to the excitation of the fundamental plasmon mode. The absorption spectra are also analyzed over wider ranges of frequencies and magnetic fields to track the resonance position.

In Fig. 2(a), we include the experimental data for the dependence of the resonance frequency on the magnetic field, measured at the gap widths of 0.25 μm (black dots) and 10 μm (blue diamonds), as compared to the unscreened 2DES disk (red squares). As one can see, in the presence of the magnetic field, the plasmon resonance splits into two branches. The low-frequency mode $\omega_-(B)$ has a negative magnetodispersion — it is often called the edge magnetoplasmon mode [17–20]. The upper mode $\omega_+(B)$, on the other hand, exhibits a positive magnetodispersion and corresponds to the usual ("bulk") 2D magnetoplasmon [9]. According to the authors of Refs. [17,21], the magnetodispersion of both modes can be expressed as

$$\omega_\pm = \pm\frac{\omega_c}{2} + \sqrt{\frac{\omega_c^2}{4} + \omega_p^2}, \tag{2}$$

where $\omega_c = eB/m^*$ is the cyclotron frequency and $\omega_p$ is the plasmon frequency at $B = 0$ at the wave vector $q = 2.4/d$ [22]. The curves calculated from Eq. (2) are plotted in solid lines in Fig. 2(a). These results make it evident that the model describes the experiment well enough to allow us to extrapolate the plasmon frequency $f_p = 18.2$ GHz at $h = 0.25$ μm. For comparison, the red squares in the figure mark the magnetodispersion measured for the unscreened 2DES disk of the same diameter 0.25 mm, with no lateral gate. Clearly,

the plasma frequency of the bare disk, $f_p = 35$ GHz, significantly exceeds the values obtained for the laterally screened 2DES structures. Physically, it can be explained by the fact that the Coulomb interaction between the charges in the plasma wave is screened by the charges induced in the gate [23–25].

For a more detailed study of the screening effect, we explored a series of samples with different sizes of the gap $h = 0.25$, 1.3, 2, 5, 7, 10, 20, and 40 μm. The resultant dependence of the plasmon frequency on the gap size is summarized in Fig. 2(b). Most interestingly, we find that no appreciable change in the plasma frequency is observed at the gap widths above 10 μm, whereas $f_p$ sharply decreases for the smaller values of $h$. To assess the validity of the findings from the physics perspective, a full-wave three-dimensional (3D) electromagnetic simulation was carried out in Ansys HFSS (for the details, see Supplementary Material [26]). The results of the numerical simulation plotted in the red line in Fig. 2(b) demonstrate a good agreement with the experimental data.

To gain more insight into the nature of the observed physical phenomenon, we develop a qualitative model. For simplicity, we can treat the plasmon in terms of the lumped element model [27–29]. In that case, a bare 2DES disk acts as a nonmagnetic inductor, with $L_K = m^*/ne^2$, connected in parallel with a capacitor of $C = 2\varepsilon_0\bar{\varepsilon}/q$, where $\bar{\varepsilon} = (1 + \varepsilon_{GaAs})/2$ is the dielectric permittivity of the medium hosting the 2DES and $q = 2.4/d$ is the wave vector specific to the disk geometry [22]. We note that such an $LC$ circuit naturally resonates at the plasmon frequency $\omega_p = 1/\sqrt{L_K C}$, in agreement with Eq. (1). In turn, the lateral screening introduces an additional capacitance $C_s$ to the given plasmonic circuit. According to the literature [30–32], the lateral capacitance can be defined as

$$C_s = \frac{2\varepsilon_0\bar{\varepsilon}}{q} \ln\frac{1}{qh}, \tag{3}$$

which results in the screened plasmon frequency

$$\omega_s(q) = \frac{1}{\sqrt{L_K(C + C_s)}} = \sqrt{\frac{ne^2q}{2m^*\varepsilon_0\bar{\varepsilon}}} \frac{1}{\sqrt{1 + \ln\frac{1}{qh}}}. \tag{4}$$

The prediction based on the proposed theoretical model is plotted in a dashed black line in Fig. 2(b). Comparing these data with the measurement and simulation results, we can see that the model captures the basic physics of the phenomenon. Namely, at the large values of the gap width $h$, the plasmon dispersion in Eq. (4) closely resembles that of the ungated 2D plasmon frequency, $\omega_p \propto \sqrt{q}$, whereas for small gaps, $qh \ll 1$, the lateral gate screening contribution increases, and the logarithmic term becomes significant. This physical picture is confirmed by the distribution of the electric fields at the plasmon resonance (inset to Fig. 3). There is a quantitative agreement between the experiment and the proposed theoretical model. Admittedly, a more elaborate theoretical model is needed for the exact description of the observed physical phenomenon, taking into account the geometrical factors. Such a model would be highly desirable for future research.

Curiously, the proposed theoretical model predicts that the normalized plasmon frequency, $\omega_s/\omega_p$, depends solely on the dimensionless parameter $qh$. Indeed, the plots of $\omega_s/\omega_p$ versus the $h/d$ in Fig. 3 demonstrate that the experimental data obtained for the disks with $d = 0.5$ mm (red squares) and $d = 0.25$ mm (black dots), at the 2DES density $n = 1.6 \times 10^{11}$ cm$^{-2}$, follow a universal functional dependence.

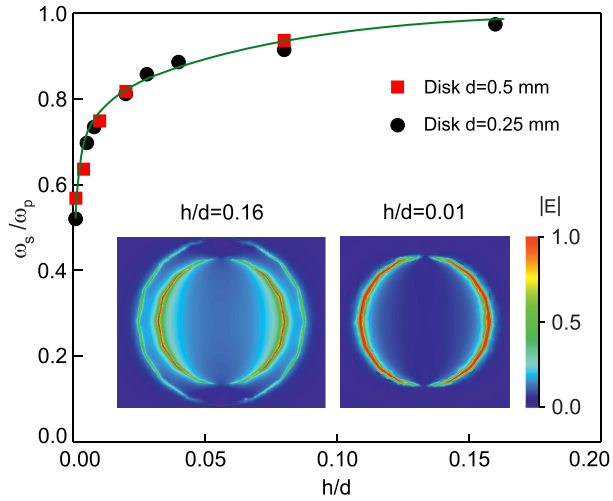


FIG. 3. Plot of the normalized plasmon frequency $\omega_s/\omega_p$ as a function of $h/d$, measured for the laterally screened 2DES disks of diameters $d = 0.5$ mm (red squares) and $d = 0.25$ mm (black dots), at the electron density $n = 1.6 \times 10^{11}$ cm$^{-2}$. The solid curve shows the result of the numerical simulation. Inset shows the color maps of field-$|E|$ distribution at the plasmon resonance for $h/d = 0.16$ and 0.01.

It is worthwhile considering what happens when $h$ tends to zero and the lateral gate is brought arbitrarily close to the 2DES edge. In real two-dimensional systems, the edge charges are accumulated in the depletion region of a finite width $l_d$. Thus, to make the results of our study applicable to realistic systems, the parameter $h$ in Eq. (4)

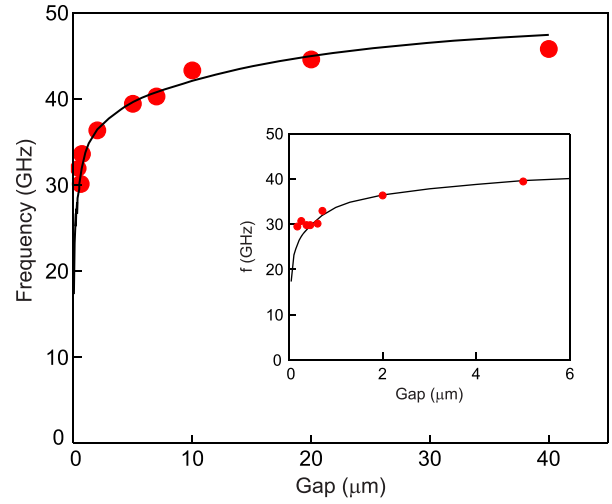


FIG. 4. The plasmon frequency plotted as a function of the gap width $h$ between the 2DES and the gate. The measurements are taken on the laterally screened 2DES disk of diameter $d = 0.25$ mm at the electron density $n = 3.5 \times 10^{11}$ cm$^{-2}$ (red dots). The solid line denotes the numerical simulation results [26]. The inset shows the plasmon frequencies on the expanded scale of the gap size, from 0.2 to 6 μm.

should be replaced with $l_d + h$. For this reason, the actual plasma frequency in Fig. 2(b) tends to a nonzero value determined by the depletion length $l_d$. Therefore, the spectroscopy of laterally screened 2D plasmons can reveal valuable details about the structure of the 2DES edge. For the sake of demonstration, we carried out a series of measurements over a finer range of the gap widths using a laterally screened 2DES disk of diameter $d = 0.25$ mm fabricated from the wafer with $n = 3.5 \times 10^{11}$ cm$^{-2}$. In the process of microfabrication, special care is taken to make the plane of the 2DES and the surface of the metal gate at the same level. Also, as can be seen in Fig. 1, the roughness of the mesa and the gate did not exceed 100 nm. As a result, Fig. 4 presents a more detailed dependency of the plasmon frequency on the gap size, where the inset shows the data on the expanded scale, from $h = 0.2$ μm to $h = 2$ μm. The experimental evidence indicates that for $h < 0.5$ μm, the plasmon frequency saturates at a constant value of 30 GHz. Consequently, we can conclude that the lateral depletion length must be approximately 0.5 μm, which is consistent with the results of previous experimental studies [33,34].

In addition to the apparent advantages of lateral gating, some difficulties may be faced during its operation. First, it is unclear how to contact the 2DES. This problem can be solved by cutting the gate segment and directing the contact pad through the resulting disclosure. Another complication is associated with gate leakage and current percolation. Using $Al_2O_3$ or Hf $O_2$ dielectrics can improve these factors. A direct demonstration of plasmon tuning by applying a gate voltage is a natural next step of current research.

In conclusion, we investigated plasma excitations in an AlGaAs/GaAs 2DES of a disk geometry, laterally screened by a gate. We found that the lateral screening leads to a significant redshift in the plasmon frequency. The theoretical model we developed and the numerical simulations show good agreement with the experimental data. We demonstrated that the spectroscopy of laterally screened plasmons provides valuable insight into the structure of the 2DES edge. Understanding the physics of lateral screening can be of critical importance in designing plasmonic detectors, generators, and phase shifters, where a grid gate is used as a tunable control electrode [35–41].

The authors gratefully acknowledge the financial support from the Russian Science Foundation Grant No. 19-72-30003.

[1] D. Tsui, S. Allen, R. Logan, A. Kamgar, and S. Coppersmithe, Surf. Sci. **73**, 419 (1978).
[2] T. N. Theis, Surf. Sci. **98**, 515 (1980).
[3] D. Heitmann, Surf. Sci. **170**, 332 (1986).
[4] J. Lusakowski, Semicond. Sci. Technol. **32**, 013004 (2017).
[5] V. M. Muravev and I. V. Kukushkin, Phys. Usp. **63**, 975 (2020).
[6] F. Stern, Phys. Rev. Lett. **18**, 546 (1967).
[7] C. C. Grimes and G. Adams, Phys. Rev. Lett. **36**, 145 (1976).
[8] S. J. Allen, Jr., D. C. Tsui, and R. A. Logan, Phys. Rev. Lett. **38**, 980 (1977).
[9] T. N. Theis, J. P. Kotthaus, and P. J. Stiles, Solid State Commun. **24**, 273 (1977).
[10] A. V. Chaplik, Zh. Eksp. Teor. Fiz. **62**, 746 (1972) [Sov. Phys. JETP **35**, 395 (1972)].
[11] V. Ryzhii, A. Satou, I. Khmyrova, A. Chaplik, and M. S. Shur, Journal of Appl. Phys. **96**, 7625 (2004).
[12] A. Satou, V. Ryzhii, and A. Chaplik, J. Appl. Phys. **98**, 034502 (2005).
[13] S. A. Mikhailov and N. A. Savostianova, Phys. Rev. B **74**, 045325 (2006).
[14] A. Satou and S. A. Mikhailov, Phys. Rev. B **75**, 045328 (2007).
[15] V. V. Popov, O. V. Polishchuk, and S. A. Nikitov, Pis'ma Zh. Eksp. Teor. Fiz. **95**, 91 (2012) [JETP Lett. **95**, 85 (2012)].
[16] I. V. Kukushkin, J. H. Smet, K. von Klitzing, and W. Wegscheider, Nature (London) **415**, 409 (2002).
[17] S. J. Allen, Jr., H. L. Störmer, and J. C. M. Hwang, Phys. Rev. B **28**, 4875(R) (1983).
[18] D. B. Mast, A. J. Dahm, and A. L. Fetter, Phys. Rev. Lett. **54**, 1706 (1985).
[19] D. C. Glattli, E. Y. Andrei, G. Deville, J. Poitrenaud, and F. I. B. Williams, Phys. Rev. Lett. **54**, 1710 (1985).
[20] V. A. Volkov and S. A. Mikhailov, Zh. Eksp. Teor. Fiz. **94**, 217 (1988) [Sov. Phys. JETP **67**, 1639 (1988)].
[21] A. Márquez and R. Esquivel-Sirvent, Opt. Express **28**, 39005 (2020).
[22] I. V. Kukushkin, J. H. Smet, S. A. Mikhailov, D. V. Kulakovskii, K. von Klitzing, and W. Wegscheider, Phys. Rev. Lett. **90**, 156801 (2003).
[23] C. Dahl, J. P. Kotthaus, H. Nickel, and W. Schlapp, Phys. Rev. B **46**, 15590(R) (1992).
[24] S. I. Gubarev, A. A. Dremin, V. E. Kozlov, V. M. Murav'ev, and I. V. Kukushkin, Pis'ma Zh. Eksp. Teor. Fiz. **90**, 588 (2009). [JETP Lett. **90**, 539 (2009)].
[25] V. Giliberti, A. Di Gaspare, E. Giovine, M. Ortolani, L. Sorba, G. Biasiol, V. V. Popov, D. V. Fateev, and F. Evangelisti, Phys. Rev. B **91**, 165313 (2015).
[26] See Supplemental Materials at http://link.aps.org/supplemental/10.1103/PhysRevB.108.115419 for details on 3D electromagnetic simulation.
[27] P. J. Burke, I. B. Spielman, J. P. Eisenstein, L. N. Pfeiffer, and K. W. West, Appl. Phys. Lett. **76**, 745 (2000).
[28] G. R. Aizin and G. C. Dyer, Phys. Rev. B **86**, 235316 (2012).
[29] V. M. Muravev, N. D. Semenov, I. V. Andreev, P. A. Gusikhin, and I. V. Kukushkin, Appl. Phys. Lett. **117**, 151103 (2020).
[30] O. G. Vendik, S. P. Zubko, and M. A. Nikolskiy, Tech. Phys. **69**, 1 (1999).
[31] G. Granet and B. Guizal, Opt. Commun. **255**, 1 (2005).
[32] O. Luukkonen, C. Simovski, G. Granet, G. Goussetis, D. Lioubtchenko, A V. Räisänen, and S. A. Tretyakov, IEEE Trans. Antennas Propag. **56**, 1624 (2008).
[33] K. K. Choi, D. C. Tsui, and K. Alavi, Appl. Phys. Lett. **50**, 110 (1987).
[34] C. Dahl, S. Manus, J. P. Kotthaus, H. Nickel, and W. Schlapp, Appl. Phys. Lett. **66**, 2271 (1995).
[35] W. Knap, Y. Deng, S. Rumyantsev, and M. S. Shur, Appl. Phys. Lett. **81**, 4637 (2002).

[36] E. A. Shaner, M. Lee, M. C. Wanke, A. D. Grine, J. L. Reno, and S. J. Allen, Appl. Phys. Lett. **87**, 193507 (2005).

[37] V. V. Popov, D. V. Fateev, T. Otsuji, Y. M. Meziani, D. Coquillat, and W. Knap, Appl. Phys. Lett. **99**, 243504 (2011).

[38] V. M. Muravev, A. A. Fortunatov, A. A. Dremin, and I. V. Kukushkin, JETP Lett. **103**, 380 (2016).

[39] A. V. Shchepetilnikov, B. D. Kaysin, P. A. Gusikhin, V. M. Muravev, G. E. Tsydynzhapov, Yu. A. Nefyodov, A. A. Dremin, and I. V. Kukushkin, Opt. Quantum Electron. **51**, 1 (2019).

[40] A. V. Shchepetilnikov, P. A. Gusikhin, V. M. Muravev, G. E. Tsydynzhapov, Yu. A. Nefyodov, A. A. Dremin, and I. V. Kukushkin, Journal of Infrared, Millimeter, J Infrared Milli. Terahz. Waves **41**, 655 (2020).

[41] V. M. Muravev, A. Shuvaev, A. S. Astrakhantseva, P. A. Gusikhin, I. V. Kukushkin, and A. Pimenov, Appl. Phys. Lett. **121**, 051101 (2022).